Physical Modeling of the Electroforming Process in Resistive-Switching Devices

A. Marchewka
Institut für Werkstoffe der Elektrotechnik II
RWTH Aachen University
52074 Aachen, Germany
marchewka@iwe.rwth-aachen.de

R. Waser and S. Menzel
Peter Grünberg Institut
Forschungszentrum Jülich
52425 Jülich, Germany
st.menzel@fz-juelich.de

***Abstract*—We present a numerical drift-diffusion model that combines bulk ionic transport with electrode kinetics for oxygen exchange to describe the electroforming process in resistive-switching devices. Simulations of electroforming by voltage ramps are conducted and the conductive filament formation is analyzed in dependence of various kinetic parameters. It is shown how the filament growth direction and the post-forming resistance state are governed by the rate of oxygen exchange compared to the rate of ionic transport inside the oxide layer.**

Keywords—ReRAM; electroforming; electrode kinetics; oxygen exchange; filament; simulation model

I. Introduction

Oxide-based resistive switches are currently attracting considerable attention as promising candidates for nonvolatile memory or logic applications [1]. The switching mechanism in these devices is widely acknowledged to rely on temperature-activated migration of donors, such as oxygen vacancies, inside the oxide and accompanying redox reactions. A related modification of the potential barrier at the electrode interfaces manifests itself in different resistance states. To activate repeatable resistance switching, an initial electroforming step is typically required. This process corresponds to a controlled soft-breakdown of the as-deposited insulating oxide, leading to the formation of localized conducting filaments and reduced device resistance. These filaments correspond to oxygen-deficient regions, which are created as oxygen is extracted from the oxide at the anodic interface [2]. Due to local Joule heating, the generated oxygen vacancies are able to migrate in the applied electric field, leading to a growth of the filament. Growth directions from the anode towards the cathode and vice versa have been observed [3, 4, 5]. Further, it has also been shown that the exchange of oxygen may take place during the switching process [6, 7]. Since the electroforming process allows controlling the filament properties and resulting device variability, a deeper understanding of the underlying physical and electrochemical mechanisms is indispensable to ensure reliable device operation. One important step on this way is the development of comprehensive simulation models. So far, a physical model that combines redox reactions at the electrodes with oxygen-vacancy transport in the oxide layer while taking into account the relevant effects of Joule heating and contact potentials has not been reported. In this work, we present such a model that allows for investigations of the interplay between electrode kinetics, oxygen-vacancy transport, and filament evolution during electroforming and resistive switching. It is used to study the impact of the oxygen-exchange rate on the formation and progression of the conductive filament during electroforming.

II. Simulation Model

A. Model geometry and system of equations

Our model is based on the drift-diffusion approach recently presented to study the reset dynamics of TaO_x-based resistive switches [8], which is extended to include the kinetics of oxygen exchange at the electrodes. The model geometry consists of a 2D axisymmetric representation (radial coordinate r, axial coordinate z, radius $R = 100$ nm) of a metal-oxide-metal structure on a substrate carrier as sketched in Fig. 1. In the initial state, the oxide layer of length $L = 10$ nm is assumed to be lightly donor-doped by oxygen vacancies of homogeneous concentration. It is bounded by a high-work-function metal electrode at $z = 0$ and a low-work-function metal electrode at $z = L$. The electronic barriers at the interfaces $z = 0$ and $z = L$ are assumed to have nominal barrier heights of $e\phi_{Bn0} = 1.8$ eV and $e\phi_{Bn0} = 0.8$ eV, respectively. Within a small radius $r = r_{fil} = 10$ nm, these barriers are assumed to be lowered, resulting in a Schottky-like contact of barrier height $e\phi_{Bn0}(r \le r_{fil},0) = 0.7$ eV at the interface $z = 0$ and an ohmic-like contact of $e\phi_{Bn0}(r \le r_{fil},L) = 0.1$ eV at the interface $z = L$. The system of partial differential equations is summarized in Fig. 1. Coupled electronic-ionic transport under nonisothermal conditions is considered by calculating the self-consistent steady-state solution of the heat equation (equation (I) in Fig. 1), Poisson equation ((II)) and electron drift-diffusion equation ((III)), followed by the calculation of a time step for oxygen-vacancy movement by solving the drift-diffusion equation for doubly ionized oxygen vacancies ((IV)) and the rate equations for the singly ionized and neutral vacancies ((V) and (VI)). To account for the effects of contact potentials, electron transport across the interface barrier via thermionic emission and tunneling is included in the model. Details on the system of equations and the solution procedure are given in [8, 9].

© 2017 The Japan Society of Applied Physics

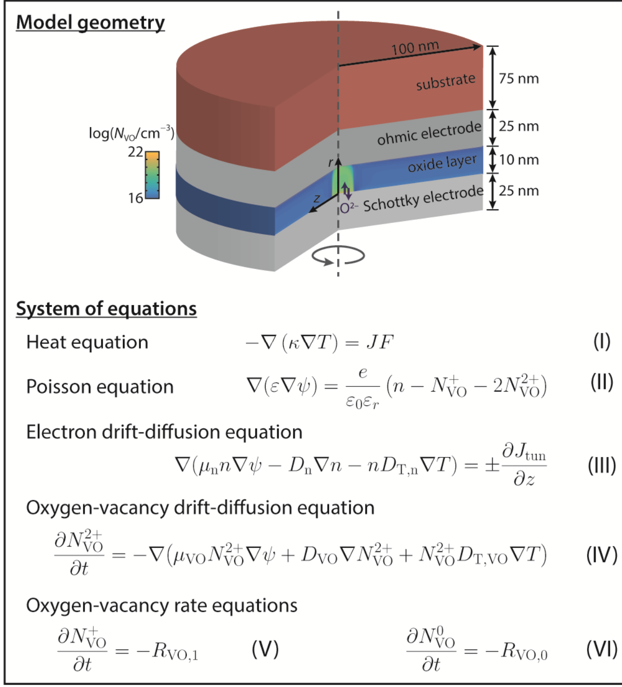

Fig. 1. Model geometry (not to scale) and system of equations. Oxygen exchange is assumed to take place within a radius $r < r_{fil} = 10$ nm at the interface between the oxide layer and the anode (Schottky-like electrode). A typcial oxygen-vacancy distribution evolving during the electroforming simulation is illustrated in the oxide layer.

B. *Modeling of oxygen exchange at the electrode*

Oxygen release and incorporation is accounted for at the Schottky-like electrode/oxide interface, while the ohmic electrode interface is assumed to block the ionic current. The oxygen-exchange reaction is assumed to take place in a confined region $r \le r_{fil}$ at $z = 0$ as indicated in Fig. 1. It is modeled using a Butler-Volmer equation for the oxygen-vacancy current density J_{VO} as boundary condition for the oxygen-vacancy drift-diffusion equation (equation (IV) in Fig. 1) according to

$$J_{VO}(r,0) = J_0(r,0)\cdot S(r)\cdot \left[\frac{N_{VO,M}(r,0)N_{O,SC}(r,0)}{N_{VO,M}^{*}N_{O,SC}^{*}}\exp\left(-\frac{\alpha z_{VO}e}{k_B T}\Delta\eta\right) - \frac{N_{O,M}(r,0)N_{VO,SC}(r,0)}{N_{O,M}^{*}N_{VO,SC}^{*}}\exp\left(\frac{(1-\alpha)z_{VO}e}{k_B T}\Delta\eta\right)\right]. \quad (1)$$

Here, J_0 is the exchange current density, $N_{O,SC}$ ($N_{VO,SC}$) the oxygen ion (vacancy) concentration in the oxide layer, $N_{O,M}$ and $N_{VO,M}$ oxygen-defect concentrations in the metal electrode, $N_{O,SC}^*$, $N_{VO,SC}^*$, $N_{O,M}^*$, and $N_{VO,M}^*$ corresponding reference concentration values, α the transfer coefficient, z_{VO} the number of involved electrons, k_B the Boltzmann constant, T the temperature, and $\Delta\eta$ the overpotential driving the reaction. The latter can be calculated from the difference between the metal Fermi level $E_{F,M}$ and the electron quasi-Fermi level in the oxide $E_{Fn,SC}$ according to

$$\Delta\eta = \frac{1}{e}\left(E_{F,M} - E_{Fn,SC}\right). \quad (2)$$

The exchange current density can be expressed as

$$J_0(r,0) = z_{VO}ek_{00}\exp\left(\frac{-\Delta G^{\circ}}{k_B T}\right)\cdot\frac{\left(N_{VO,M}^{*}N_{O,SC}^{*}\right)^{1-\alpha}}{\left(N_{O,M}^{*}N_{VO,SC}^{*}\right)^{-\alpha}} \quad (3)$$

with k_{00} being the reaction-rate constant and ΔG° the Gibbs free energy of activation under standard conditions. The logistic function is chosen as

$$S(r) = \left(1 + \exp\left(-1\times10^{10}\,\mathrm{m}^{-1}\cdot(r - r_{fil})\right)\right)^{-1} \quad (4)$$

to produce a smooth decrease of the exchange current density around $r = r_{fil}$. As oxygen is extracted from the oxide layer by passing the oxide/electrode boundary, it is transferred to the electrode region. The Schottky-like electrode is treated to act as an oxygen reservoir that can receive and release oxygen ions. Neglecting thermodiffusion and the voltage drop across the electrode, the oxygen-ion distribution is simulated by solving the diffusion equation for oxygen ions

$$\frac{\partial N_{O,M}}{\partial t} = -\frac{1}{z_O e}\nabla\cdot J_O = \nabla\cdot\left(D_O\nabla N_{O,M}\right) \quad (5)$$

in the electrode region. Here, J_O denotes the oxygen-ion current density, z_O denotes the charge number, and D_O the diffusion coefficient. The ionic flux at the oxide boundary is opposite to the vacancy flux given by (1) and thus obeys

$$J_O(r,0) = -J_{VO}(r,0). \quad (6)$$

No oxygen exchange is assumed to take place with the surrounding atmosphere, i.e. $J_O(r,z = -25\text{ nm}) = 0$.

III. Simulation Results

A. *Variation of the rate constant k_{00}*

Simulations of the electroforming procedure are conducted to study the impact of the oxygen-exchange rate on the formation and progression of the conductive filament. Initially, a homogeneous donor concentration $N_{VO} = 1\times10^{16}$ cm^{-3} is assumed in the oxide layer, and no oxygen ions are assumed to be present in the Schottky-like electrode. A voltage ramp of rate 4 V/s is applied to the device, and the simulation is stopped after a current increase to 300 µA or more has been achieved. Fig. 2(a) shows the simulated *I-V* characteristics for oxygen exchange rates between $k_{00} = 1\times10^{-34}$ cm^4/s and $k_{00} = 1\times10^{-22}$ cm^4/s, corresponding to exchange current densities $J_0 = 5.8\times10^{-17}$ A/m^2 and $J_0 = 5.8\times10^{-5}$ A/m^2. A strong increase in current over more than 10 orders of magnitude is observed for all curves. The curves of high exchange rates exhibit a sudden strong increase in current and a clear forming voltage can be identified as indicated for $k_{00} \le 1\times10^{-22}$ cm^4/s in Fig. 2(a). For low exchange rates $k_{00} \le 1\times10^{-31}$ cm^4/s, the

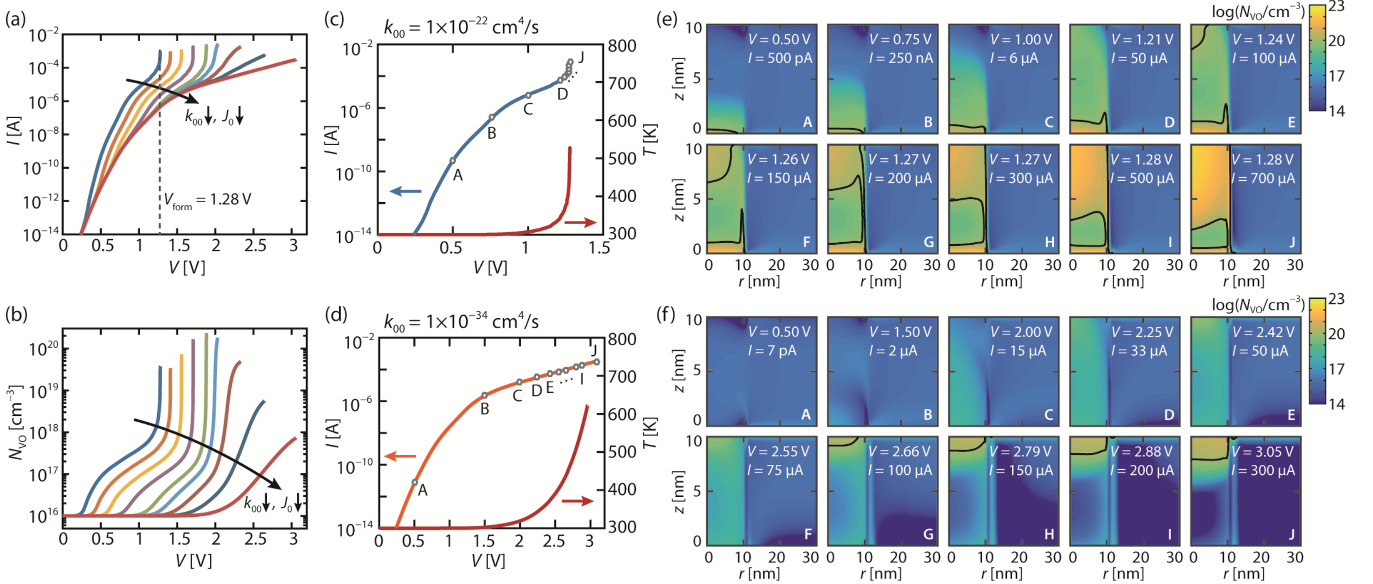

Fig. 2 (a) I-V characteristics for different oxygen-exchange rates k_{00} during a voltage ramp, (b) evolution of the average donor concentration in the oxide layer, (c) evolution of current and maximum temperature for k_{00} =°10^{-22} cm^4/s, (d) evolution of current and maximum temperature for k_{00} =°10^{-34} cm^4/s, (e) maps of the oxygen-vacancy concentration at points A to J as marked in the I-V characteristics in (c), (f) maps of the oxygen-vacancy concentration at points A to J as marked in the I-V characteristics in (d). The black line in the concentration maps marks the isoline of N_{VO} = 1×10^{20} cm^{-3} and illustrates the filament evolution.

current increase is rather smooth and limited by the internal series resistance of the device, rendering the determination of a unique forming voltage impossible. The increase in current is related to the continuous increase in oxygen-vacancy concentration in the oxide layer, which is shown in Fig. 2(b). The increase in oxygen-vacancy concentration already starts at low voltages and currents, where significant Joule heating does not yet take place. As the current increases, the associated temperature rise exerts a positive feedback on the oxygen-exchange rates. For large exchange rates, a thermal runaway occurs, manifesting itself in the abrupt current and concentration increase, accompanied by an abrupt increase of temperature, as shown in Fig. 2(c) for k_{00} = 1×10^{-22} cm^4/s. For low exchange rates, this runaway does not occur, and the increase in concentration is rather gradual. Fig. 2(d) shows the corresponding gradual behavior of the temperature evolution for a low rate of k_{00} = 1×10^{-34} cm^4/s. A more detailed analysis of the evolution of the oxygen-vacancy concentration is provided by the maps in Fig. 2(e) and (f), showing the concentration distribution within a radius r = 30 nm at different points in time A to J as marked in Fig. 2(c) and (d), respectively. Referring to Fig. 2(e), the high reaction rate constant of k_{00} = 1×10^{-22} cm^4/s leads to an increase in oxygen-vacancy concentration already at voltages below 0.5 V, where self-heating does not yet occur. The filament starts growing from the anode (Schottky-like contact at z = 0), where the oxygen vacancies are introduced, towards the cathode (ohmic-like contact at z = L), cf. snapshots A to D in Fig. 2(e). When temperature increases and the donors become mobile, they drift towards the cathode and start accumulating there as evident from snapshots E and F. The increase in overall oxygen-vacancy concentration leads to a self-acceleration of the oxygen exchange and the oxygen-vacancy migration due to increased Joule heating. The accumulation region at the anode further grows into direction of the cathode interface as can be seen from snapshots G to J. Still, there is also an accumulation of oxygen vacancies at the anode interface as oxygen exchange sustains, delivering new vacancies at that interface. For the reaction rate constant k_{00} = 1×10^{-32} cm^4/s, cf. Fig. 2f, the oxygen-vacancy concentration starts to slowly increase from V = 2 V onwards, where the temperature is already slightly elevated, cf. Fig. 2(d). The oxygen vacancies introduced at the anode interface are therefore able to immediately drift towards the cathode interface, where they subsequently accumulate as can be seen in snapshots D to J. In contrast to the previous example, no significant accumulation takes place at the anode interface z = 0, and the filament grows from the cathode interface at z = L into the direction of the anode. Here, a region depleted of oxygen vacancies remains at the Schottky-like interface, resulting in a relatively large potential barrier further limiting the current and the temperature rise. The positive feedback of including additional vacancies is thus reduced, and the electroforming procedure is less abrupt than for the opposite filament growth direction. Another reason for the smooth behavior is related to the series resistance of the oxide layer, which is determined by the electron concentration inside the oxide layer. Due to a higher contact barrier and lower donor density, the electron concentration is lower, corresponding to a higher series resistance. Thus, a considerable amount of the applied voltage drops across the oxide layer, and an increase in voltage has only a minor impact on the resulting overpotential at the contact interface that drives the exchange reaction.

B. *Variation of the activation energies for the oxygen-exchange reaction and oxygen-vacancy migration*

The previous results show that filament formation and progression is governed by two concurrent processes, i.e. oxygen-vacancy incorporation and oxygen-vacancy migration.

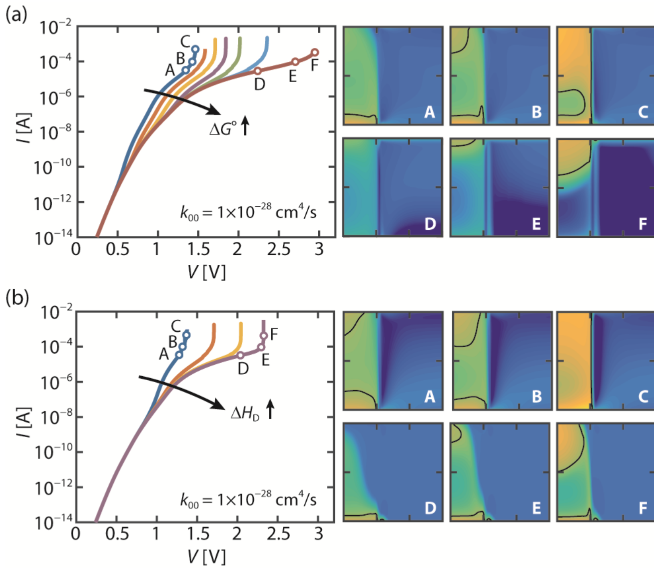

Fig. 3 (a) *I-V* characteristics for $\Delta G°$ varied between 0.6 eV and 1.2 eV in steps of 0.1 eV and maps of the oxygen-vacancy concentration showing the filament evolution for the lowest and highest value of $\Delta G°$; (b) *I-V* characteristics for ΔH_D varied between 0.75 eV and 0.9 eV in steps of 0.05 eV and maps of the oxygen-vacancy concentration showing the filament evolution for the lowest and highest value of ΔH_D.

According to (3), the oxygen-exchange rate exhibits an exponential temperature dependence with the activation energy $\Delta G°$. Oxygen-vacancy migration is linked to the oxygen diffusion coefficient, which is assumed to obey the Arrhenius law with a migration enthalpy ΔH_D. It is modelled as

$$D_{VO} = D_0 \exp\left(-\frac{\Delta H_D}{k_B T}\right)\left(1 - \frac{N_{VO}^{2+}}{N_{VO,max}}\right), \quad (7)$$

where D_0 is the diffusion-coefficient prefactor, $N_{VO}{}^{2+}$ the concentration of doubly-ionized oxygen vacancies, and $N_{VO,max}$ the maximum possible oxygen-vacancy concentration in the oxide layer. Depending on the activation energy of both processes and the temperatures during the forming process, the ratio between the oxygen exchange rate and the rate of oxygen transport in the bulk oxide layer might change, leading to different filament formations. Fig. 3(a) shows the simulated *I-V* characteristics for different values of the Gibbs free energy of activation $\Delta G°$ ranging from 0.6 eV to 1.2 eV (steps of 0.1 eV). Similar as in the k_{00} variation study, the *I-V* behavior shows a steep increase in current if the oxygen-exchange rate is high, i.e. $\Delta G°$ is low, which turns into a gradual behavior for lower exchange rates, i.e. large $\Delta G°$. Here, $k_{00} = 1 = 1\times10^{-28}$ cm^4/s was chosen. With increasing $\Delta G°$, the onset of the thermal runaway is delayed and the associated forming voltage increases. The concentration maps shown for the lowest and highest value of $\Delta G°$ reveal that the abrupt increase is accompanied by a filament growth from the anode towards the cathode, while the gradual behavior occurs for the opposite growth direction. The influence of the oxygen-vacancy migration enthalpy on the *I-V* characteristics is shown Fig. 3(b) for ΔH_D varied between 0.75 eV and 0.9 eV in steps of 0.05 eV. Here, a thermal runaway leading to an abrupt current increase is observed for $\Delta H_D \geq 0.8$ eV, i.e. low diffusion rates. For $\Delta H_D = 0.75$ eV, the steep increase in current is rather attributed to fast oxygen-vacancy diffusion inside the oxide, leading to a quite homogeneous distribution in the filament, than to increased temperatures. The concentration maps on the right show the evenly distributed oxygen vacancies for the low value of ΔH_D forming a cylindrical filament, while for high ΔH_D the oxygen vacancies remain at the anode for longer time. The low diffusion rate also implies a radial broadening of the oxygen-vacancy distribution at the anode interface, leading to a more conically shaped filament.

IV. Conclusion

In summary, an advanced numerical model is presented that includes all main physical and electrochemical mechanisms involved in resistive switching and electroforming. Simulations of filament formation during the electroforming process show that the filament growth direction and the post-forming resistance state are governed by the rate of oxygen exchange compared to the rate of ionic transport inside the oxide layer.

References

[1] J. J. Yang, D. B. Strukov, and D. R. Stewart, "Memristive devices for computing", *Nat. Nanotechnol.*, vol. 8, pp. 13-24, 2013.

[2] J. J. Yang et al., "The mechanism of electroforming of metal oxide memristive switches", *Nanotechnology*, vol. 20, pp. 215201, 2009.

[3] E. Yalon et al., "Detection of the insulating gap and conductive filament growth direction in resistive memories", *Nanoscale*, vol. 7, no. 37, pp. 15434-15441, 2015.

[4] H. Du et al., Chem. Mater., "Nanosized conducting filaments formed by atomic-scale defects in redox-based resistive switching memories", *Chem. Mater.*, vol. 29, pp. 3164-3173, 2017.

[5] D. Kalaev, E. Yalon, and I. Riess, "On the direction of the conductive filament growth in valence change memory devices during electroforming", *Solid State Ionics*, vol. 276, pp. 9-17, 2015.

[6] W. Kim et al., "Impact of oxygen exchange reaction at the ohmic interface in Ta_2O_5-based ReRAM devices", *Nanoscale*, vol. 8, no. 41, pp. 17774-17781, 2016.

[7] D. Cooper et al., "Anomalous Resistance Hysteresis in Oxide ReRAM: Oxygen Evolution and Reincorporation Revealed by in situ TEM", *Advanced Materials*, vol. 29, no 23, pp. 1700212, 2017.

[8] A. Marchewka et al., "Nanoionic Resistive Switching Memories: On the Physical Nature of the Dynamic Reset Process", *Adv. Electron. Mater.*, vol. 2, pp. 1500233, 2016.

[9] A. Marchewka, R. Waser and S. Menzel, "Physical Simulation of Dynamic Resistive Switching in Metal Oxides Using a Schottky Contact Barrier Model," *International Conference On Simulation of Semiconductor Processes and Devices (SISPAD),* pp. 297-300, 2015.